information

MDPI

Article

DTWICA: A Novel Method for Constructing Character Templates in Imaginary Handwriting

Jiaofen Nan [1], Panpan Xu [1,2], Gaodeng Fan [1], Xueqi Jin [1], Shuyao Zhai [1], Yanting Li [1], Yongquan Xia [1], Yinghui Meng [1], Liqin Yue [2,*] and Duan Li [1,*]

[1] School of Computer Science and Artificial Intelligence, Zhengzhou University of Light Industry, Zhengzhou 450001, China; nanjiaofen@zzuli.edu.cn (J.N.); 332305090551@zzuli.edu.cn (P.X.); 332305080532@zzuli.edu.cn (G.F.); 332405100505@zzuli.edu.cn (X.J.); 332405070485@zzuli.edu.cn (S.Z.); 2019027@zzuli.edu.cn (Y.L.); 2007023@zzuli.edu.cn (Y.X.); yinghuimeng@zzuli.edu.cn (Y.M.)

[2] Faculty of Engineering, Huanghe Science and Technology College, Zhengzhou 450000, China

* Correspondence: yueliqin@hhstu.edu.cn (L.Y.); liduan@hpu.edu.cn (D.L.)

Abstract

Imaginary handwriting is an important research paradigm in the field of brain-controlled typing. Neural signals exhibit high complexity, low signal-to-noise ratio, and strong temporal and environmental variability, leading to significant inter-trial differences in the temporal dynamics of character-related signals. These factors pose significant challenges for segmenting character-related signals and accurately decoding imaginary handwriting. To address these issues, this study proposes a Dynamic Time Warping Independent Component Analysis (DTWICA) framework. This framework employs FastDTW to construct individualized warping functions for each trial, followed by FastICA-based decomposition to separate the signal into distinct temporal and neuronal factors. The decomposed temporal factors are then mapped and transformed using the warping function and subsequently merged with the neuronal factors to reconstruct the signal. A sliding time window is then applied for adaptive processing, yielding the transformed signal. Finally, the transformed signals from multiple trials are averaged to generate a template for each character. Results based on a publicly available neural signals dataset for imaginary handwriting indicate that, compared with mainstream time warping models such as Shift, Linear, Piecewise, and TWPCA, the proposed model improves the character decoding accuracy for 31 characters by 14%, 13%, 7%, and 2%, respectively. This study not only constructs effective character signal templates but also facilitates accurate character segmentation during unlabeled imagined typing in an offline setting, providing a promising methodological basis for future real-time imagined typing decoding systems.

Keywords: brain-computer interface (BCI); imaginary handwriting; character template; time warping; cross-trial alignment

Check for updates

Academic Editor: Anirban Bandyopadhyay

Received: 7 March 2026
Revised: 13 April 2026
Accepted: 14 April 2026
Published: 17 April 2026

Copyright: © 2026 by the authors. Licensee MDPI, Basel, Switzerland. This article is an open access article distributed under the terms and conditions of the Creative Commons Attribution (CC BY) license.

1. Introduction

Imaginary handwriting is a communication method based on neural recordings [1], which enables text input without limb movement by recognizing brain activity during imagined spelling. Compared to spelling paradigms based on motor imagery (MI) [2] or steady-state visual evoked potential (SSVEP) [3], imaginary handwriting offers a higher information transfer rate and a more natural interaction modality [4,5]. However, due to the high dimensionality of neural recordings and the temporal variability across individuals and trials [6–8], the decoding accuracy and stability of imaginary handwriting remain

challenging [9]. Mapping and deforming neural signals of the same character across different trials to construct standardized signal templates is crucial for distinguishing character classes during imagined handwriting-based typing.

Neural signal templates are standardized feature representations from characteristic signal patterns [10,11], which are widely used for signal alignment and decoding optimization in BCI systems [12]. In imaginary handwriting tasks, different users or different trials from the same user may exhibit significant temporal shifts [13]. Even for the same imagined character, neural responses can vary dynamically across trials [14]. Such temporal variability can lead to instability in template matching, affecting character recognition accuracy. Therefore, effectively aligning the temporal dynamics of character-related signals and extracting stable neural patterns are key to neural signal template construction [15]. Signal alignment techniques rely on effective time warping methods [16]. The core of time warping methods lies in developing an appropriate mapping strategy to stretch and adjust signals, thereby eliminating temporal misalignment across trials of the same task.

Currently, time warping alignment techniques can be categorized into three main types: distance-based time warping, feature-based time warping alignment, and deep learning-based time warping alignment. Distance-based alignment methods achieve alignment by computing and optimizing the distance between data sequences. It mainly obtains a mapping relationship through the calculation of the minimum distance, enabling different time series to be aligned or matched in a certain sense [16]. Dynamic Time Warping (DTW), as a classical time-series alignment technique, minimizes the distance between sequences by allowing nonlinear mappings and is widely used in speech recognition, handwriting recognition, financial data analysis, and neuroscience. In 1985, Huang et al. [17] first applied DTW to EEG analysis. In EEG analysis, DTW can adaptively align signals with non-uniform speed variations and temporal delays, but it faces challenges such as unstable alignment paths, high computational complexity, and sensitivity to noise when handling high-dimensional and large-scale data. To address these issues, researchers have proposed various improvements. Feng et al. [18] proposed Generalized Canonical Time Warping, which integrates DTW with Canonical Correlation Analysis for joint alignment of multimodal data. Zhao et al. [19] introduced Shape Dynamic Time Warping, which enhances the semantic consistency of alignment by incorporating local structural information. Soheily-Khah et al. [20] proposed Sparsified-Paths search space DTW, which reduces computational cost by sparsifying the alignment path. Additionally, Hong et al. [21] proposed Shape Segment Dynamic Time Warping, which refines time segment division using wavelet transforms to improve alignment accuracy. These studies provide diverse solutions for the application of DTW in high-dimensional time series analysis, promoting its widespread use in neuroscience and pattern recognition.

Feature-based alignment methods achieve alignment by adjusting key features in the signal, such as time, frequency, and amplitude, enabling alignment between different trials or signals, and are widely used in neuroscience and signal processing. Chemin et al. [22] proposed a time warping method for EEG, which adjusts non-strictly periodic EEG signals through time scaling and frequency domain analysis to improve the analysis of rhythm-related neural responses. Williams et al. proposed Time Warped Principal Components Analysis (TWPCA) [23], which uses Singular Value Decomposition to extract the low-dimensional temporal and neuronal structures of neural data, modeling inter-trial temporal variations. To deal with the problem of the insufficient adaptability of traditional models to the changes of local details, a generalized linear and piecewise linear time warping framework was proposed [24], improving the flexibility of time warping modeling by dynamically estimating phase and frequency variations across multiple trials. However, its limitation lies in its dependence on task templates, which restricts its generalization

capability to unknown tasks. To meet the need for transfer learning across tasks, Song et al. [25] proposed an alignment method based on P300 signals, which uses latency, amplitude, and inversion factors to achieve cross-dataset signal transformation, significantly improving transfer learning accuracy and demonstrating strong generalization ability. The aforementioned studies provide multi-level solutions in the field of high-dimensional signal time alignment, laying a solid foundation for neural data analysis.

In recent years, deep learning-based time-series alignment techniques have demonstrated great potential in cross-domain data analysis. The core idea is to introduce neural network models that automatically learn time warping features, enabling more precise signal alignment and analysis [26,27]. By integrating deep learning techniques such as convolutional neural networks [28,29], recurrent neural networks [30], attention mechanisms [31], and autoencoders [32], a fully automated process has been achieved, covering feature learning to time warping modeling. With continuous advancements in technology, these methods exhibit greater robustness and generalization capabilities in nonlinear signal alignment, cross-trial and cross-dataset signal alignment, and large-scale data processing.

In summary, distance-based warping alignment algorithms are well suited for signals with temporal continuity and sequential dependencies, effectively handling nonlinear temporal variations within signals s [33]. However, the main drawbacks of DTW lie in its high computational complexity and sensitivity to noisy data [27]. Feature-based warping alignment methods offer strong interpretability, but they are highly dependent on the definition of the mapping function and are susceptible to model selection biases. Deep learning-based alignment methods can capture complex dynamics in multi-dimensional time series, but they suffer from poor interpretability and high training costs. Therefore, this study integrates distance-based and feature-based warping alignment methods and proposes a Dynamic Time Warping Independent Component Analysis (DTWICA). The main contributions of this work are as follows:

(1) This study proposes a character template construction method for neural signals based on DTWICA. By optimizing the signal decomposition and mapping processes, this approach enhances the accuracy and stability of neural signal during imaginary handwriting.
(2) This method dynamically captures temporal similarities across trials by accounting for time shifts and phase jitter in neural signals. It constructs an optimal time warping function for each trial to obtain time mapping parameters.
(3) This method employs Fast Independent Component Analysis (FastICA) to separate temporal and neuronal factors. The obtained time mapping parameters are applied to the temporal factors, and after reintegrating with the neuronal factors, the transformed neural signals are generated. A sliding time window is then used for adaptive discrimination, producing the warped neural signals for character representation.
(4) We conducted a systematic evaluation of the DTWICA model on a publicly available dataset. The results demonstrate that this method outperforms existing mainstream approaches in terms of classification accuracy, F1 score, and other evaluation metrics, validating its effectiveness and superiority.

2. Materials and Methods

2.1. Datasets

This study used the publicly available handwriting BCI dataset released by Willett et al. [23] from Stanford University (https://datadryad.org/dataset/doi:10.5061/dryad.wh70rxwmv, accessed on 11 April 2026). This dataset records neural activity from a participant with severe spinal cord injury, who had two 96-channel Utah microelectrode arrays (Utah MEAs [34]) implanted in the precentral gyrus of the brain. The participant was

paralyzed below the neck, with hand movements limited to slight twitches and motions. The experiment required the participant to imagine holding a pen and writing letters and symbols in response to instructions displayed on a computer screen. This dataset includes neural recordings of the participant during imagined handwriting of both single characters and sentences. We utilized the single-character neural dataset to construct character templates. The dataset contains 26 lowercase English letters and five special characters (comma, apostrophe, question mark, period, and space), which serve as pause markers during imagined handwriting sentences. Given that neural signals generated when imagining handwriting of spaces and periods are weak and difficult to capture, the experiment instructed the participant to use the greater-than symbol ('>') to represent spaces and the tilde ('~') to represent periods. Figure 1 presents the reconstructed handwriting trajectory decoded from neural signals corresponding to the imagined handwriting of 31 characters.

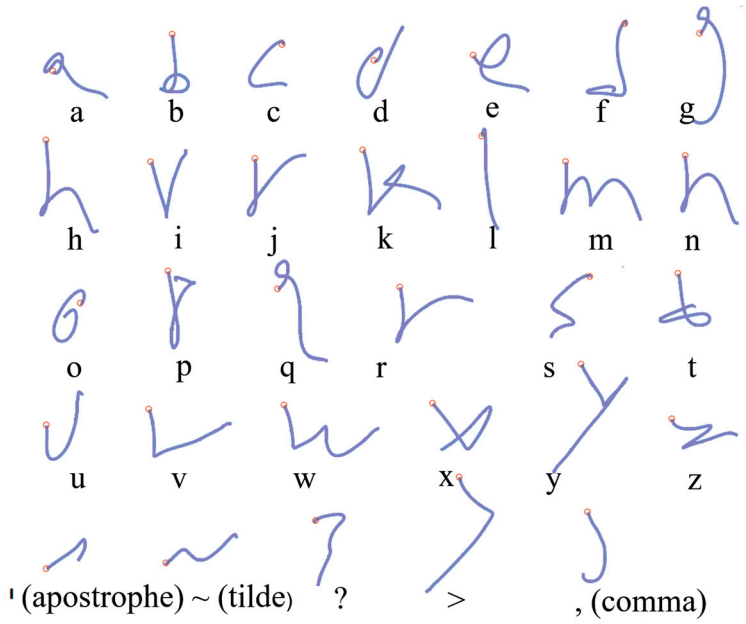


Figure 1. Example of decoded handwriting trajectories for 31 imagined characters. The red circles indicate the starting points of the trajectories.

This study primarily constructs character templates based on neural signals during imagined handwriting of single characters and evaluates their classification accuracy using a KNN classifier. To comprehensively assess the performance of the constructed character templates, the study applies the constructed character templates to segment the imagined handwriting sentence into characters. The neural recordings contain 1000 sentences, each of which is preprocessed into a 1200 × 192 matrix, where 1200 represents the number of time points and 192 denotes the number of electrodes.

2.2. Overall Architecture

To effectively construct character templates for neural signals and evaluate their performance, the process in this study is divided into three main stages: preprocessing, template construction, and template evaluation, as illustrated in Figure 2.

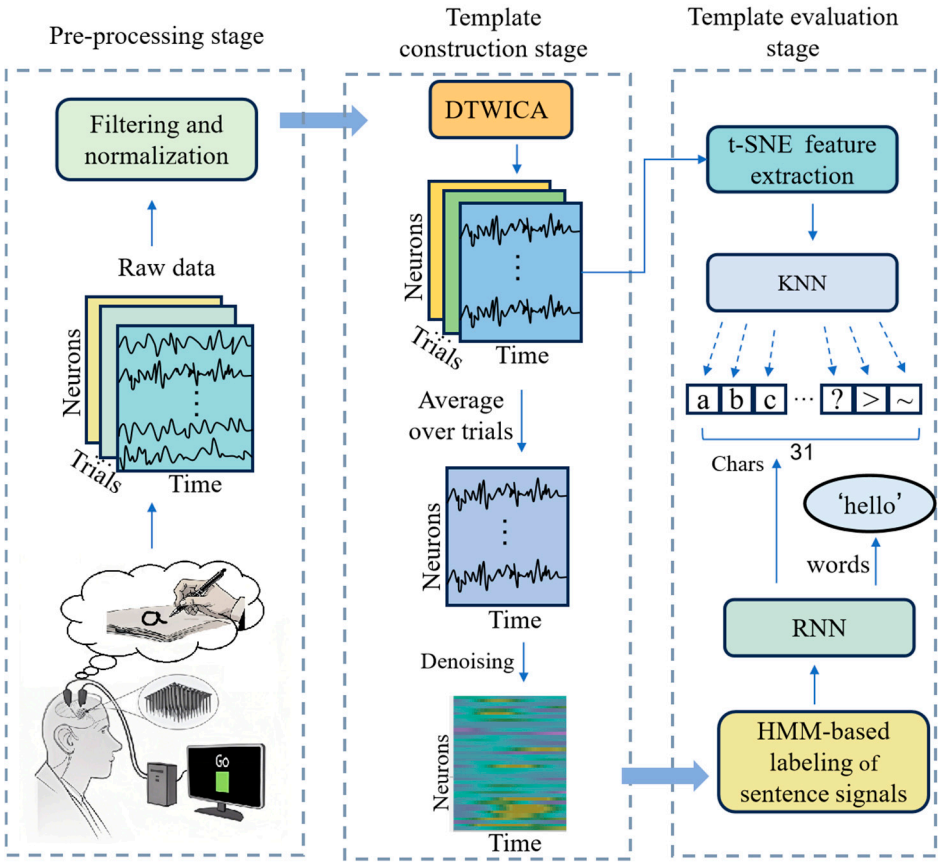


Figure 2. Overview of the framework.

2.2.1. Preprocessing Stage

After acquiring the data, a common-mode reference filter was first applied to subtract the average signal across the neural recording array from each electrode signal, thereby reducing common-mode noise. Subsequently, a band-pass filter (250–3000 Hz) was applied to each neural channel, followed by threshold crossing detection. To compensate for baseline firing-rate drift over time and inter-channel amplitude differences, the firing rate of each neuron was normalized using z-score normalization, as shown in Equation (1), where, X_k^n represents the data from the k-th trial sample (k = 1, 2, 3, . . ., 837) for the n-th neuron, and $\overline{X}_n$ denotes the mean of all trials for the n-th neuron. The neural activity data were then smoothed along the temporal dimension using a Gaussian filter (Python 3.13 using SciPy (version 1.1.0)) with a standard deviation of 3 to control the degree of smoothing.

$$z_n = \frac{X_k^n - \overline{X}_n}{\sqrt{\frac{1}{n}\sum_{i=1}^{n}\left(X_k^n - \overline{X}_n\right)^2}} \quad (1)$$

2.2.2. Template Construction Stage

Due to temporal differences across trials, DTWICA is used to align these trials to a shared temporal space, allowing neural signals from different trials to be compared and analyzed within the same time framework. DTWICA constructs a time warping function for each trial using FastDTW and applies FastICA to perform matrix decomposition on the signals, obtaining temporal and neuronal factors. The time warping function is applied to the temporal factors of each trial, which is then combined with the neuronal factors to form the warped signal. Then, the reconstruction error between the warped signal and the original data is calculated to construct the loss function, and the warping function, temporal factors, and neuronal factors are iteratively updated using the Adam optimizer.

Subsequently, further processing with a sliding time window results in the appropriately warped signal for the window. The overall DTWICA framework is shown in Figure 3 and can be roughly divided into three stages: signal alignment, iterative optimization, and sliding time window processing.

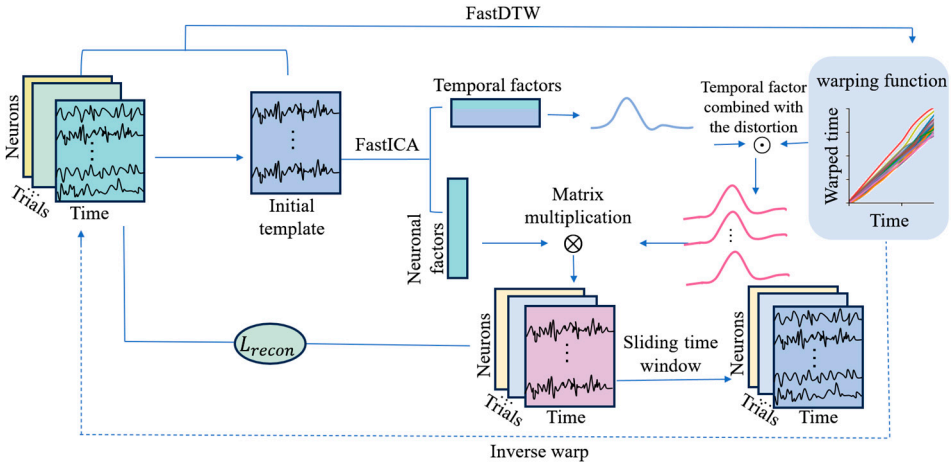


Figure 3. DTWICA Framework.

Signal Alignment: FastDTW is used to initialize the warping function f and perform the initial time alignment of the data. Specifically, the mean of all trials for a single-character dataset is computed to obtain the initial template $\overline{X}$. Then, FastDTW is used to compute the path relationship between the neural activity of each trial and the initial template, obtaining the relative temporal offsets and constructing the warping function f for each trial. Finally, the warping function f is applied to the original data, resulting in the initially aligned data. The core idea of this process is to compute the similarity between each trial and the initial template using the dynamic programming algorithm of FastDTW, and build the warping function accordingly. FastDTW efficiently aligns two time series through multi-scale approximation and local search windows. Its core operation involves aligning the time series at a coarse resolution to obtain an approximate matching path. Then, the path is refined at higher resolutions to narrow the alignment range. Finally, the process is recursively performed layer by layer until the alignment is completed at the original resolution. The process is as follows:

(1) Coarsening: The input time series is downsampled, reducing its length to a fraction of the original data in order to construct a coarse alignment path.

(2) Rough Alignment: Standard DTW is performed between each trial and the initial template according to Equation (2) to obtain an approximate matching path. Here, the input data $X_k \in R^{t \times n}$ represents the neural activity of the k-th trial with t time points and n neurons. $Dist(i,j) = \left|\left|X_k[i] - \overline{X}[j]\right|\right|$, both i and j are indices of time points.

$$D(i,j) = Dist(i,j) + \min[D(i-1,j), D(i,j-1), D(i-1,j-1)] \quad (2)$$

(3) Path Projection: The rough alignment path is projected onto the time series X_k and $\overline{X}$ at the original resolution, forming a search window to limit the search space for precise alignment.

(4) Refinement: Local DTW is performed within the search window obtained from the projection to optimize the final mapping relationship, resulting in the initially aligned data Xa.

Each trial contains 201 time points and 192 channels of neural activity signals. Next, the preliminarily aligned data Xa are subjected to FastICA matrix decomposition to obtain

the initial temporal factors T and neuronal factors N, as shown in Equation (3). FastICA is a widely used blind source separation algorithm designed to extract statistically independent components from multidimensional signals. Its core is to use non-Gaussianity as a measure of independence and extract independent components by maximizing negentropy. In this study, FastICA is employed to extract latent independent components from neural activity data and decompose them into T and N. The specific steps are as follows:

$$Xa \approx T * N^T \tag{3}$$

(1) Whitening process: To ensure the stability and performance of the algorithm, the data are first centered using Equation (4). Next, the centered data is whitened using Equation (5) to transform its covariance matrix into an identity matrix. First, the covariance matrix of the data is computed and decomposed into eigenvectors and eigenvalues. Then, the data are standardized by applying the inverse square root of the eigenvalues, resulting in the whitened data Xw. Here, E represents the eigenvector matrix, and D represents the eigenvalue matrix.

$$Xc = Xa - mean(Xa) \tag{4}$$

$$Xw = X_C E D^{-\frac{1}{2}} E^T \tag{5}$$

(2) Initialize Weight Vector: A weight vector w_v is randomly initialized for each latent independent component, where v = 1, 2, 3, …, V, and $V = 5$ in this study, which is used to iteratively extract independent components.

(3) Nonlinear optimization: The core of the Fast ICA algorithm is iterative optimization using nonlinear functions to achieve the separation of T and N. Non-Gaussianity measures (such as using the tanh or u3 nonlinear activation functions) are used to optimize each extracted independent component, updating the weight vector, as shown in Equation (6). Here, y = $Xw \times w_v$ is the signal obtained by projecting with the weight vector, and g is the nonlinear function.

$$w_{new_v} = E[X_w^T g(y)] - E[g'(y)]w_v \tag{6}$$

where E represents the eigenvector matrix.

Then, the updated weight vector is normalized. To ensure that the extracted components are linearly independent, the linear components of the already extracted components are removed by orthogonalization after each update, and the weight vector is normalized to unit length. The above optimization steps are repeated until the change between the new and old weight vectors is smaller than a set threshold, and at this time the algorithm is considered to have converged, and the iteration is stopped.

The temporal factors are computed as $T = X_w W$, $T \in R^{201\times5}$, W represents the final extracted mixing weight matrix. The neuronal factors are obtained as $N = W^{-1}$, $N \in R^{192\times5}$. These factors reveal the latent independent sources within the signal, corresponding to temporal dynamic patterns and neuronal spatial patterns, respectively. To ensure that the temporal and neuronal factors have the same scale, they are rescaled according to Equations (7) and (8), respectively.

$$T = \frac{T * \sqrt{\| T \|_2 * \| N^T \|_2}}{\| T \|_2} \tag{7}$$

$$N = \frac{N * \sqrt{\| T \|_2 * \| N^T \|_2}}{\| N \|_2} \tag{8}$$

Here, $\| * \|_2$ denotes the Euclidean norm for each column of the factor matrix.

Iterative Optimization: The Adam optimizer is used to alternately optimize and update the neural factor N, the time factor T, and the time warping function f. Using the current f and T, the warped time factor $f(T)$ is obtained, and the reconstructed data predicted by the model is computed, which can be expressed by Equation (9), where $\hat{X}_k$ represents warped reconstructed signal.

$$\hat{X}_k = f(T) * N^T \tag{9}$$

The reconstruction error L_{recon} of the neural signals is constructed as the objective function according to Equation (10), where $\lambda * R(f)$ controls the smoothness of the time warping, and the initial value of f is set to 0.001 to prevent overfitting. Then, the gradients of the loss function with respect to T, N, and f are calculated, and the temporal factors T, neuronal factors N, and time warping function f are updated, as shown in Equations (11)–(13), where η is the learning rate set to 10-3. This process is repeated until the loss function converges or the maximum number of iterations (1000) is reached.

$$L_{recon} = \sum_{k=1}^{n_{trials}} \left\| X_k - \hat{X}_k \right\|_F^2 + \lambda * R(f) = \sum_{k=1}^{n_{trials}} \| f(T) * N^T - X_k \|_F^2 + \lambda * R(f) \tag{10}$$

$$T^{(n+1)} = T^{(n)} - \eta \frac{\partial L_{recon}}{\partial T} \tag{11}$$

$$N^{(n+1)} = N^{(n)} - \eta \frac{\partial L_{recon}}{\partial N} \tag{12}$$

$$f^{(n+1)} = f^{(n)} - \eta \frac{\partial L_{recon}}{\partial f} \tag{13}$$

Sliding Time Window Processing: The warped reconstruction data $\hat{X}_k = \{x_1, x_2, \ldots, x_t\}$ is processed using a sliding window to further obtain a more standardized neural signal. Here, x_t represents the data collected at the t-th time point. By setting the window size c and the window step size s, the number of windows m is obtained, as shown in Equation (14). Here, $\lfloor . \rfloor$ denotes the floor function. Temporal features within the window are extracted using the sliding step, resulting in the final warped signal.

$$m = \left\lfloor \frac{\mathrm{t} - c}{\mathrm{s}} \right\rfloor + 1 \tag{14}$$

After processing with DTWICA to obtain the corresponding character's time-warped data, the mean of all trials is first calculated along the trial dimension to obtain a more standardized neural signal, i.e., the constructed character signal template. We compute the average value at each time point and for each neuron, ignoring NaN values to eliminate individual differences between trials. Next, we perform one-dimensional Gaussian filtering along the time dimension to smooth the time series and reduce noise. Subsequently, the data is fed into Principal Component Analysis (PCA) for training, reducing the dimensionality of the neural activity. The reduced data will be reconstructed into the original space, but only the first 10 principal components will be retained, thereby reducing noise and removing less-contributing components. After these processing steps, a character template is obtained, which will provide high-quality template data for subsequent signal analysis and classification tasks.

2.2.3. Template Evaluation Stage

(1) Evaluation Process

After the time alignment processing using the DTWICA framework, the warped neural activity features were directly used for KNN classification to evaluate the character decoding performance. A 10-fold cross-validation strategy was adopted, in which 90% of the samples were used as the training set and the remaining 10% as the testing set in each fold. The average classification accuracy was obtained across all ten folds. In addition, t-Distributed Stochastic Neighbor Embedding (t-SNE) was separately performed only for two-dimensional visualization of feature clustering and class separability. The perplexity parameter, which controls the balance of local data structures, was set to 20. It should be noted that the t-SNE embeddings were used solely for visualization and were not involved in the KNN classification process.

Additionally, the character templates are applied to the partition of sentences based on the Hidden Markov Model (HMM) [35], and the classification performance of words, and sentences is evaluated using a Recurrent Neural Network (RNN).

It should be noted that this character-level KNN experiment is designed primarily to validate the effectiveness of the constructed templates for downstream sentence segmentation, rather than to serve as a strict generalization benchmark.

(2) Evaluation Metrics

This study primarily evaluates the template performance using accuracy, recall, precision, and F1 score. Accuracy measures the proportion of correctly predicted samples out of the total number of samples, as shown in Formula (15); Precision measures the proportion of true positive samples among the samples predicted as positive by the model, as shown in Formula (16); Recall represents the proportion of true positive samples that the model correctly identifies among all actual positive samples, as shown in Formula (17); F1 score is the harmonic mean of precision and recall, providing a comprehensive reflection of the model's overall performance, as shown in Formula (18).

$$Accuracy = \frac{TP + TN}{TP + TN + FP + FN} \tag{15}$$

$$Precision = \frac{TP}{TP + FP} \tag{16}$$

$$Recall = \frac{TP}{TP + FN} \tag{17}$$

$$F1 = \frac{2 \times Precision \times Recall}{Precision + Recall} \tag{18}$$

where TP stands for True Positive, FN for False Negative, TN for True Negative, and FP for False Positive.

Each target character class was sequentially defined as the positive class, while the remaining 30 classes were collectively treated as the negative class. The corresponding TP, TN, FP, and FN metrics were then calculated independently for each class. Finally, by applying the above binary evaluation procedure to all 31 classes separately, the performance of the overall multi-class classification task was comprehensively quantified. In this study, Precision, Recall, and F1 are computed for each class and then macro-averaged across all classes. All results are based on the average through cross-validation.

3. Result

3.1. Effect of the Warping Function on Character Template

Since the warping function plays a crucial role in DTWICA, we compared the separability of characters before and after warping. The results are shown in Table 1. The average accuracy of 10-fold cross-validation without time warping was 53.44%. After applying FastDTW to construct the warping function, the average accuracy was increased to 93.45%. It can be observed that after applying the warping function constructed by FastDTW to deform the signals, the average accuracy was improved by approximately 40%, demonstrating the importance of the warping function in brain decoding different character categories.

Table 1. Introduction of Datasets.

	Unwarped	**FastDTW-Warped**
Accuracy (%)	53.44 ± 6.20	**93.45 ± 1.71**

Note: Bold text indicates best results.

We further visualized the neural activity during the imagined handwriting process before and after time warping, as shown in Figure 4. Compared to the neural activity of individual trials without time warping, the neural activity after time warping showed a clear alignment trend. Moreover, for the original data not processed by the DTWICA model, the neural activity of 27 trials for the character "a" was lightly stable within a time range for the first two independent components, while for independent components 3 to 5, the neural activity exhibits a more chaotic pattern, increasing the complexity of subsequent decoding operations. After warping, a clear peak alignment trend was observed for all five independent components. This indicated that even though the neural activity became more chaotic with an increasing number of independent components, FastDTW was still able to capture complex neural signals and achieve more refined trial alignment, demonstrating the effectiveness of the model proposed in this study.

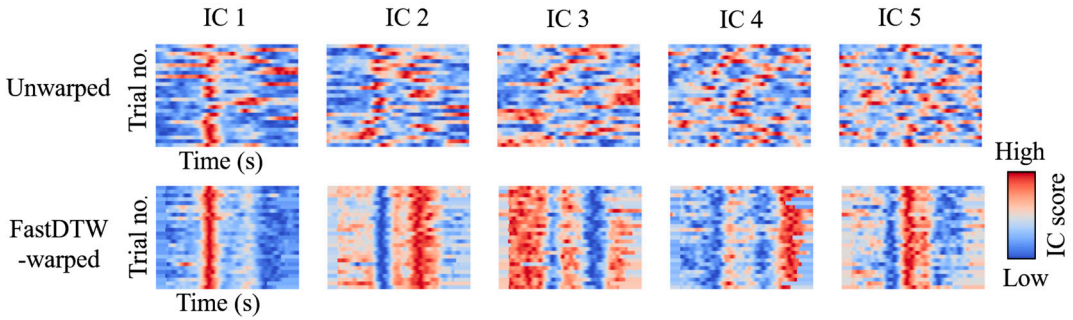


Figure 4. Neural activity of the first five independent components across different trials during imagined handwriting of the character "a". IC score represents the activation level of each independent component at a specific time point.

3.2. Effect of Signal Decomposition Methods on Character Template

Keeping the overall framework of this study unchanged, we individually replaced the signal decomposition methods and obtained the template accuracy for 31 characters, as shown in Figure 5. Regardless of the decomposition method used, the classification accuracy of characters exceeded 90%, demonstrating the effectiveness of the overall framework. Furthermore, our proposed method achieved the highest character classification accuracy (94.31%), outperforming other decomposition methods. Specifically, PCA achieved a classification accuracy of 94.21%, which is close to but slightly lower than that of FastICA.

The classification performance of Factor Analysis (FA, 93.61%), Dictionary Learning (DL, 93.57%) and TruncatedSVD (93.45%) is quite comparable. In comparison, the TCA method achieved the lowest classification accuracy but still reached 91.6%.

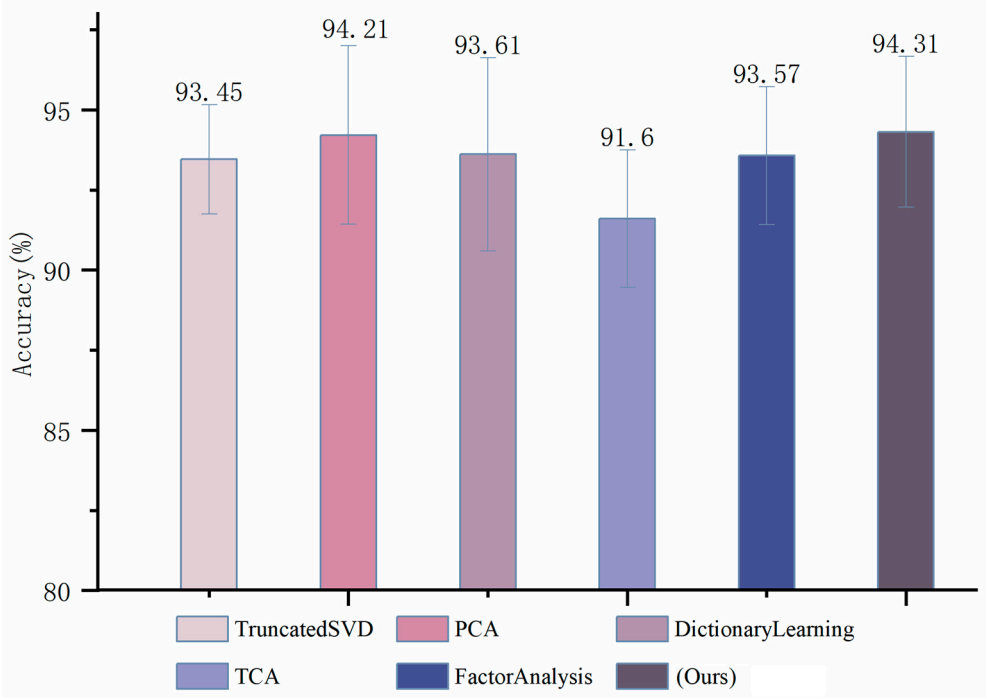


Figure 5. Effect of Matrix Decomposition Methods on Character Template Accuracy.

3.3. Effect of Sliding Time Window on Character Template

After applying time warping to the signals, we performed sliding window processing, selecting appropriate window sizes to remove the unrelated noise. Figure 6 illustrates the impact of different window sizes on template accuracy. Across six signal decomposition methods, we found that the optimal window size for DTWPCA (FastDTW + PCA), DTWDL (FastDTW + DL), DTWTCA (FastDTW + TCA), and DTWFA (FastDTW + FA) was 191 time points, whereas DTWSVD (FastDTW + TruncatedSVD) and our proposed method achieved optimal performance with a window size of 181 time points. Our method not only exhibited faster convergence but also achieved the highest classification accuracy among all methods, with an average accuracy of 94.39% under ten-fold cross-validation. Additionally, we further investigated the effect of the sliding step size on the signal when using a window size of 181 time points (see Table 2). As the sliding window moved, the character classification accuracy gradually declined.

Table 2. Effect of Sliding Step Size on Character Template.

Acccuracy (Mean ± STD) / Methods	Time Window Range (ms)				
	[0, 181]	**[5, 186]**	**[10, 191]**	**[15, 196]**	**[20, 201]**
DTWSVD	93.88 ± 1.43	91.93 ± 3.87	89.92 ± 3.46	89.40 ± 4.12	88.66 ± 3.07
DTWPCA	92.38 ± 3.04 *	92.33 ± 2.88	90.90 ± 3.26	90.42 ± 3.18	87.65 ± 1.98
DTWDL	93.76 ± 2.77	91.96 ± 3.06	91.27 ± 2.99	90.74 ± 2.95	88.24 ± 2.54
DTWTCA	90.86 ± 2.05 ***	89.67 ± 2.65	88.10 ± 3.14	86.65 ± 4.55	83.87 ± 4.24
DTWFA	92.66 ± 3.30 *	93.03 ± 3.08	91.31 ± 4.11	89.77 ± 3.31	88.15 ± 2.66
Ours	**94.39 ± 2.63**	92.06 ± 3.27	90.86 ± 2.97	89.94 ± 4.38	86.56 ± 2.99

Note: * $p < 0.05$, *** $p < 0.001$, Bold text indicates best results.

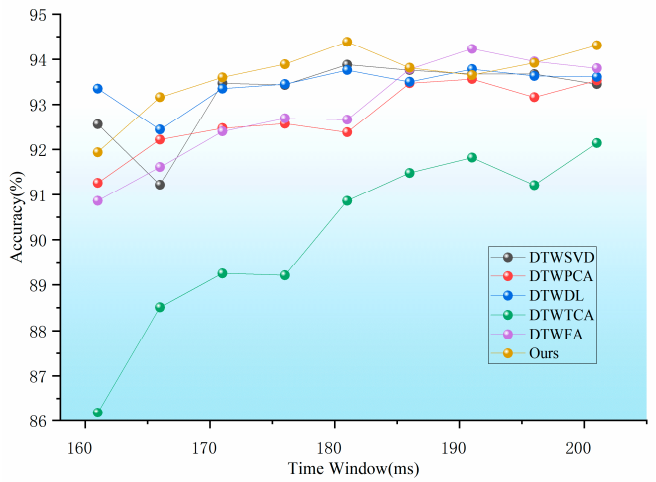


Figure 6. Effect of Sliding Time Window Size on Character Template.

3.4. Comparison with Mainstream Time Warping Techniques

To evaluate the performance of the proposed method, we compared it with four mainstream time warping methods, as shown in Table 3. The classification accuracy of neural signals without time alignment was the lowest (53.44% ± 6.20%), confirming that temporal variability significantly impacts character template classification. After applying the Shift and Linear methods, the accuracy improved to 79.47% ± 3.95% and 81.47% ± 4.29%, respectively, demonstrating that basic temporal adjustments could partially reduce errors. The Piecewise method further optimized the time alignment process and achieved 87.79% ± 3.59%, which represented a 6.32% improvement over the Linear method and highlights the advantage of nonlinear alignment approaches. The TWPCA method, which combined time warping alignment and signal decomposition, enhanced classification accuracy to 92.73% ± 3.75%, showing the benefit of integrated feature extraction and temporal correction. Notably, our proposed method achieved the highest classification accuracy (94.39% ± 2.63%) with the smallest error margin, confirming its superiority in temporal dynamic correction and its effectiveness in neural classification.

Table 3. Effect of Warping Function on Character Template.

Methods	Unwarped	Shift	Linear	Piecewise	TWPCA	Ours
Accuracy (%)	53.44 ± 6.20	79.47 ± 3.95	81.47 ± 4.29	87.79 ± 3.59	92.73 ± 3.75	**94.39 ± 2.63**

Note: Bold text indicates best results.

To further validate the effectiveness of the proposed method, we conducted t-SNE visualization to analyze the feature clustering performance of different warping approaches (Figure 7). The unwarped data (Figure 7a) exhibited poor clustering characteristics, with features widely dispersed and significant inter-class overlap, roughly forming four major clusters corresponding to character groups with similar stroke patterns (“m”, “n”, “h”), enclosed structures (“o”, “b”, “p”), and similar shapes (“l”, “i”). While both Shift (Figure 7b) and Linear (Figure 7c) methods improved intra-class compactness to some extent, they fail to achieve satisfactory inter-class separation. The Piecewise method (Figure 7d) shows enhanced discriminability but still struggles with certain character pairs. TWPCA (Figure 7e) further improved class boundaries and feature compactness, though some challenging pairs like “x”/”y” and “d”/”o” remain overlapping. In contrast, our proposed method (Figure 7f) demonstrated superior performance, effectively separating these easily confusable character pairs while maintaining excellent intra-class cohesion, thereby validating its effectiveness in the time warping alignment method.

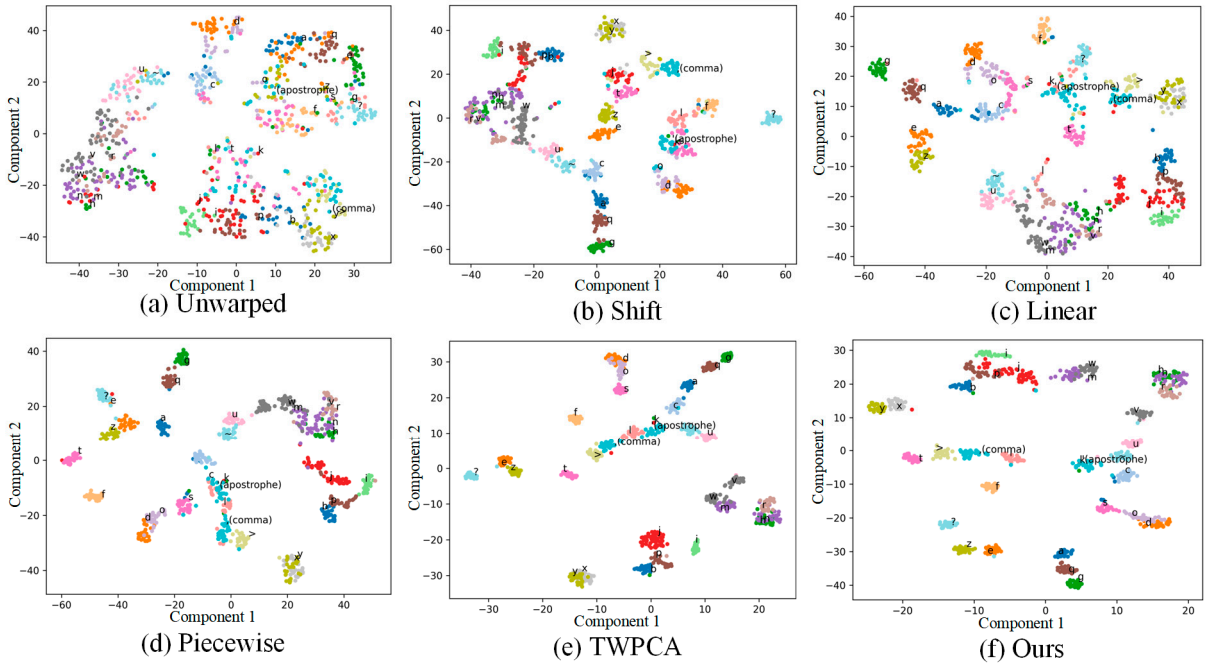


Figure 7. 2D t-SNE Visualization of Neural Activity for Different Time Warping Alignment Methods.

To comprehensively assess different alignment strategies, we analyzed confusion matrices (Figure 8). The baseline method without time warping (Figure 8a) demonstrated significantly inferior performance compared to other approaches. Application of the Shift method (Figure 8b) yielded substantial improvement, with 13 characters achieving perfect recall (1.0). The Linear method (Figure 8c) further enhanced performance, enabling 16 characters to reach full recall, though the character "h" remains problematic with a low recall of only 0.2. The Piecewise method (Figure 8d) showed incremental progress, improving the recall of "h" to 0.4 while maintaining other characters' performance. TWPCA (Figure 8e) represented a notable advancement, with 21 characters attaining perfect recall, although "h"'s recall persists at 0.4. Our proposed method demonstrated consistent improvements across multiple challenging characters ("h", "j", "k", "m", "n", "o", "x", ">", ","), despite minor regressions (e.g., "b" decreasing from 1.0 to 0.88). The experimental results conclusively demonstrated our model's superior robustness and classification performance across diverse character recognition tasks.

To rigorously assess the method's robustness, we conducted a focused analysis on five frequently confused characters ("h," "k," "m," "n," and "o"). Table 4 demonstrates that our proposed method yielded substantial improvements across all three evaluation metrics for these challenging cases compared to unwarped data. Notably, the proposed approach outperforms all competing methods in distinguishing these confusable characters, with TWPCA showing comparatively inferior performance.

Table 4. Comparison of Recall, Precision, and F1 Score for Five Easily Confused Characters.

Characters	Metrics	Methods					
		Unwarped	**Shift**	**Linear**	**Piecewise**	**TWPCA**	**Ours**
h	Recall	0.20	0.20	0.20	0.40	0.40	**0.57**
	Precision	0.09	0.25	0.20	0.33	**0.40**	0.33
	F1-score	0.12	0.22	0.20	0.36	0.40	**0.42**
k	Recall	0.00	1.00	0.80	0.80	0.80	**1.00**
	Precision	0.00	0.71	0.80	1.00	0.67	**0.83**
	F1-score	0.00	0.83	0.80	0.89	0.75	**0.91**

Table 4. *Cont.*

Characters	Metrics	Methods					
		Unwarped	**Shift**	**Linear**	**Piecewise**	**TWPCA**	**Ours**
m	Recall	0.43	0.71	0.71	0.57	0.86	**0.88**
	Precision	0.60	0.71	0.56	0.44	1.00	**1.00**
	F1-score	0.50	0.71	0.63	0.50	0.92	**0.94**
n	Recall	0.25	0.50	0.50	0.25	0.50	**0.56**
	Precision	0.50	0.57	0.67	0.67	**1.00**	0.67
	F1-score	0.33	0.53	0.57	0.36	**0.67**	0.61
o	Recall	0.50	0.88	**1.00**	**1.00**	0.88	0.91
	Precision	1.00	0.88	0.89	**1.00**	1.00	**1.00**
	F1-score	0.67	0.88	0.94	**1.00**	0.94	0.95

Note: Bold text indicates best results.

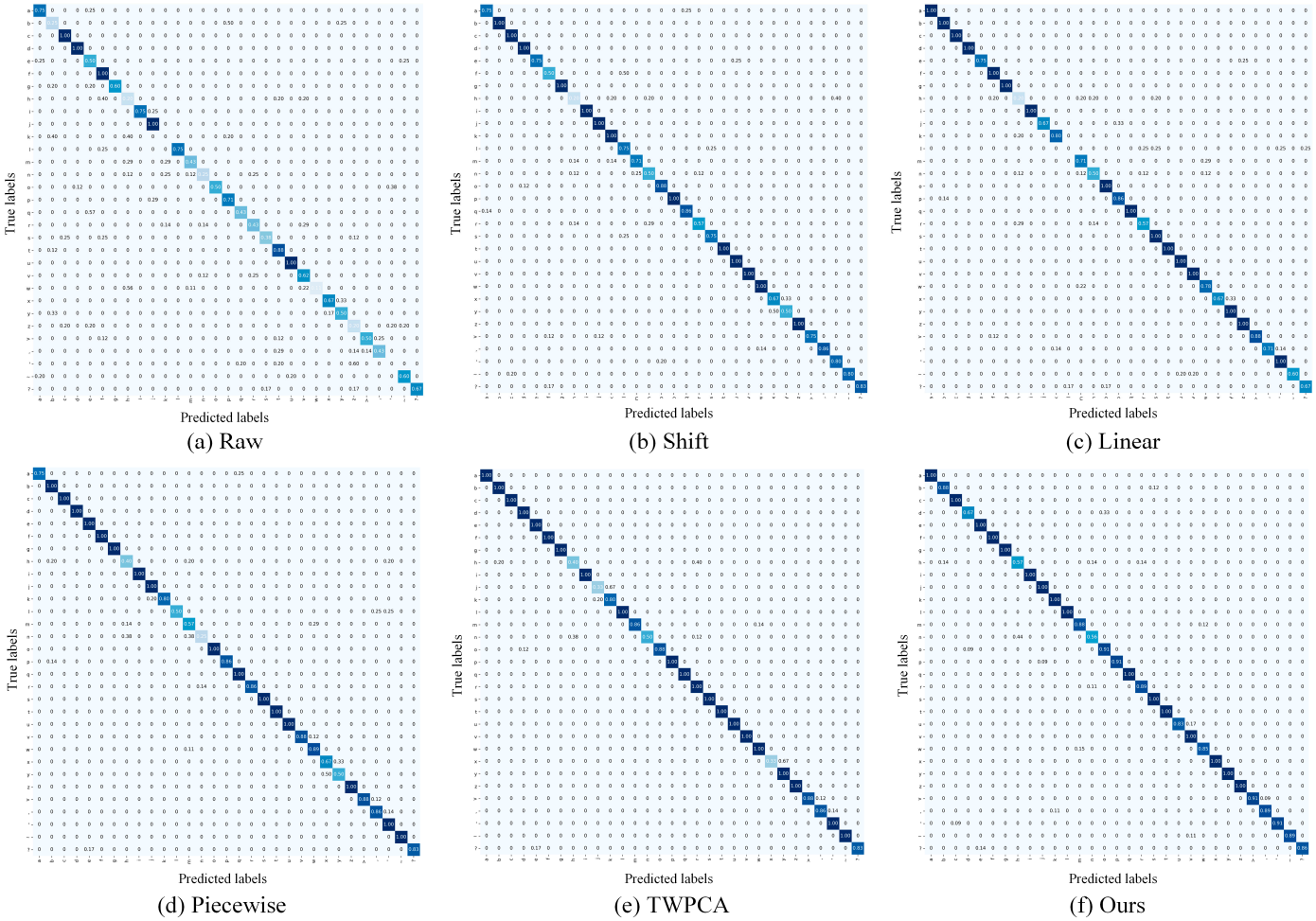


Figure 8. Confusion Matrices Under the KNN Classifier. The values in the confusion matrix represent the recall rate of each character, ranging from 0 to 1. The darker the color, the closer it is to 1; the lighter the color, the closer it is to 0.

Building upon the demonstrated superiority in character decoding accuracy of both our proposed method and TWPCA, we extended their application to sentence-level decoding tasks. In this implementation, we employed a HMM framework to perform sentence signal segmentation using the learned character templates. This process transformed the character-level signals within sentences into a one-hot encoded probability matrix, which was then utilized as input for training and classification within a RNN architecture. The experimental results presented in Table 5 reveal that our proposed method

achieved a 2.11% improvement in word recognition accuracy and an 8.76% enhancement in sentence recognition accuracy compared to the TWPCA, thereby conclusively validating the efficacy of character templates for sentence segmentation tasks. These results provided a solid foundation for developing real-time neural decoding systems for imagined handwriting applications.

Table 5. Application Effect of Character Templates in Sentence Segmentation.

Models	Word Accuracy (%)	Sentence Accuracy (%)
TWPCA [23]	85.76	25.40
Ours	**87.87**	**34.16**

Note: Bold text indicates best results.

4. Discussion

We present a general time-warping-based framework for constructing character signal templates, which autonomously discovers precise temporal patterns in neural data through an unsupervised, data-driven approach, effectively extracting representative signal templates for imagined handwriting of individual characters. Leveraging these templates, our method achieves a classification accuracy of 94.39% on the imagined handwriting single-character dataset using KNN. For the imagined handwriting sentence dataset, the system attains word-level and sentence-level classification accuracies of 87.87% and 34.16%, respectively, when employing RNN-based classification.

4.1. Neurocognitive Basis of Character-Specific Neural Variability

Imagined handwriting neural signals refer to the intracortical neural activity elicited when a participant performs the motor imagery process of handwriting characters without producing any actual limb movement [36]. This process is essentially an advanced form of motor imagery, involving multi-level neural cognitive activities ranging from character representation to the generation of complex writing trajectories. During imagined handwriting, the brain first performs visual and semantic representation of the target character at a higher cognitive level. Subsequently, at the motor planning level, the writing trajectory is internally organized and activates neural networks that are highly associated with actual handwriting movements, including the primary motor cortex, supplementary motor area, premotor cortex, and parietal-related regions [37]. The coordinated activity of these regions is reflected as recordable neural signals through changes in synaptic potentials. Although no actual muscle contraction occurs, this neural activation pattern exhibits a high degree of similarity to real handwriting in terms of both temporal structure and spatial distribution. From the perspective of signal generation, imagined handwriting neural signals are not the output of a single neural source; rather, they are the superimposed result of neuronal population activities across multiple functional regions. Along the temporal axis, these signals reflect dynamic changes at key stages such as writing initiation, stroke transition, and writing termination. Therefore, different characters can evoke temporally distinguishable neural patterns during imagined handwriting, which provides the physiological basis for neural based character recognition and decoding.

4.2. Effect of Time Warping Functions

This study constructs warping functions based on FastDTW to effectively address nonlinear alignment issues in neural signals. Experimental comparisons demonstrate that its performance surpasses existing mainstream methods. It is well known that changes in environment and mental or physical state can cause variations in how an individual processes the same event [38]. Similarly, when the same subject imagines handwriting the

same character, different trials of neural signals often exhibit temporal misalignment and morphological variations. The traditional Shift method only applies a simple translation to the signal, which can partially alleviate temporal misalignment but does not account for complex variations in brain signal morphology [24]. The Linear method allows for global linear stretching and compression of the signal, considering both temporal shifts and morphological differences in brain signals. However, it applies a uniform transformation across all trials of the same task. In contrast, the Piecewise is more flexible, introducing segmentation nodes to apply localized transformations within the same trial, allowing both translation and deformation of the signal. Originally developed for neuroscience applications, it has been used to study behavioral decoupling and inter-trial temporal variations [24]. The above techniques directly deform the original signals, whereas the TWPCA model is fundamentally different. It introduces signal decomposition before deformation, using the decomposed temporal signals combined with the Shift technique to achieve temporal translation, thus avoiding unreasonable deformation of spatial domain information. Currently, brain-controlled typing is mainly achieved through decoding multi-channel data, which not only relies on temporal features of brain signals but is also closely related to spatial and phase features. Based on this, this study further improves the TWPCA model, primarily by using factor decomposition methods combined with FastDTW to deform brain signals, thereby achieving high consistency across different trials of the same character. FastDTW is an optimized version of DTW, primarily aligning each trial with an initial template, calculating the time offset for each trial through multi-scale approximation and local search window strategies, and applying this to each trial's signal to complete the signal deformation [39]. This method not only takes into account the nonlinear correction of temporal features but also addresses the issue of preserving the integrity of spatial features, thereby solving the problem of over-correction caused by nonlinear warping.

4.3. Effect of Decomposition Methods

Neural signals encompass multi-dimensional information such as temporal, frequency, and spatial domains [40]. Direct time warping of the entire signal may lead to abnormal changes in features from other dimensions. Therefore, it is crucial to decompose independent temporal factors from signals. There are many decomposition methods for signals, such as TruncatedSVD, PCA, DL, TCA, FA, and FastICA. TruncatedSVD is based on Singular Value Decomposition, retaining only the top k largest singular values and their corresponding singular vectors to achieve dimensionality reduction [41]. In this decomposition framework, the top k left singular vectors form the temporal factors, while the right singular vectors correspond to the neuronal factors. However, TruncatedSVD primarily focuses on the global structure of the data and has limitations when handling local features in signals. PCA computes the covariance matrix and performs eigenvalue decomposition [42], extracting the top k eigenvectors with the largest variance as neuronal factors. The original data is projected onto this feature space to obtain temporal factors. PCA assumes the data is linearly separable and cannot effectively handle the nonlinear features in signals, thus having limitations in capturing complex temporal dynamics. DL learns a set of dictionary elements, enabling signals to be represented as a sparse linear combination [43]. The optimization process of DL alternates between updating the dictionary matrix and the sparse coding matrix, with the final dictionary matrix and sparse coding matrix corresponding to the temporal factors and neuronal factors, respectively. DL effectively extracts sparse features from signals but cannot handle high-dimensional representations of signals effectively. TCA decomposes high-dimensional data tensors into the product of multiple low-dimensional tensors, minimizing reconstruction error

by optimizing the objective function, thereby obtaining the final temporal factors and neuronal factor [44]. However, TCA does not explicitly optimize the separability between dimensions, making it difficult to ensure that the decomposed temporal and neuronal factors have strong discriminative power. FA assumes that observed data consists of a linear combination of latent factors plus noise, decomposing the signal into the product of a factor loading matrix and a factor score matrix, with an error term added [45]. The temporal factors and neuronal factors are formed by the final optimized factor loading matrix and factor score matrix. The goal of FA is to maximize the variance explained, but due to its focus on the covariance structure of the data, it has limited adaptability to nonlinear signals. As shown in Figure 5, among the methods discussed, PCA performs the best, followed by DL, then FA, TruncatedSVD, and TCA in sequence. In contrast, the current study uses FastICA to decompose high-dimensional signals, removing irrelevant artifacts and extracting independent temporal and spatial features. FastICA first centers and whitens the data, then optimizes the iterative process based on non-Gaussianity metrics to maximize the independence of the decomposed components. The neuronal factors are formed by the independent components of FastICA, while the temporal factors are obtained through the projection of the signals onto the space. signals have high-dimensional complexity and non-Gaussian properties, while FastICA can extract independent temporal patterns from complex data, reduce aliasing effects, and ensure that temporal factors can decouple the signals more precisely during time alignment, thus improving alignment accuracy. At the same time, FastICA can remove artifacts such as eye movements and muscle activity, ensuring that the alignment focuses primarily on the relevant brain signals associated with imagined handwriting, rather than noise. This is the reason why the temporal factors obtained using FastICA in this study are superior.

4.4. Effect of Sliding Time Window

After warping and transforming the decomposed temporal factors and re-integrating them with the neuronal factors, the time axes of each trial are roughly synchronized. However, using a fixed window length may fail to fully extract temporal features and lead to resource waste, making it difficult to construct refined signal templates for each character. In contrast, the sliding time window not only further isolates noise but also allows independent processing of the signal within each window [46]. Generally, even after time alignment, signals may still contain complex temporal variations. For instance, some dynamic features (such as periodic waveforms or non-stationarity) may manifest as changes over short periods of time for signals. By using a sliding time window, the model can more accurately capture these dynamic features in the temporal domain, thereby improving classification performance. As shown in Figure 7 and Table 2, the adaptive sliding time window can select the optimal window length. In addition, appropriate window settings help improve character template, allowing the model to process large-scale data in a shorter amount of time.

4.5. Limitations and Future Perspectives

In practical BCI systems, robustness to noise and inter-session variability remains a well-recognized challenge. Neural signals may vary substantially across different recording sessions due to signal drift, electrode condition changes, user fatigue, fluctuations in mental state, and environmental differences, all of which can significantly affect decoding stability and system reliability [38]. To address this issue in real-world deployment, the BCI framework proposed in this study is designed to adopt a daily personalized calibration strategy. That is, before each use of the system, the participant first completes a character imagery practice task. Based on the neural signals collected from this practice, a subject-

specific character recognition template is built for that day. Then, in subsequent online tasks such as actual spelling and mental communication, this daily personalized character template serves as the basis for classification and decoding, enabling stable mental character output and communication based on the day's calibration data.

Notably, although the sentence-level accuracy is only 34.16%, errors in individual characters can be effectively corrected by incorporating a large language model. After integrating the Bigram LM large language model, the decoded sentences achieved an accuracy of 71%, making it possible for practical application.

Despite these promising results, several limitations remain. First, the template constructed in this study has not fully explored other dimensional information such as the frequency domain and spatial domain. Secondly, due to differences in individual writing habits and environmental variability, there may be significant differences in neural activation patterns among different subjects. Thirdly, the current manuscript does not provide neurophysiological validation, which is an important direction for future work.

5. Conclusions

Due to temporal variations in neural signals caused by physiological, psychological, and external factors during repeated execution of the same character in brain typing, significant challenges exist in both segmenting character-level signals and achieving accurate imagined typing decoding. To address this issue, this study proposes a DTWICA-based character signal template construction method, which effectively builds character-specific signal templates and facilitates character segmentation from continuous imagined typing sentences in an offline setting. These results provide a promising methodological basis for future online and real-time imagined typing decoding systems.

Author Contributions: J.N., writing—review and editing, supervision, and validation; P.X., writing—original draft, methodology, and data curation; G.F., formal analysis and conceptualization; X.J., validation and conceptualization; S.Z., formal analysis and conceptualization; Y.L., conceptualization and software; Y.X., conceptualization and investigation; Y.M., investigation and resources; L.Y., investigation and resources; D.L., formal analysis and software. All authors have read and agreed to the published version of the manuscript.

Funding: This work was supported by the key Science and Technology Program of Henan Province [262102211079, 262102211027 and 252102210139], the National Natural Science Foundation of China [No. 82370513 and No. 62476255], Research and Application of Key Technologies for High-Precision Large Dynamic Unmanned Aerial Vehicle Power Inspection Electro-Optical Pod [No. 252102210002], the Key Science Research Project of Colleges and Universities in Henan Province of China [No. 25A520003], Post-Doctoral Foundation of Henan Province [No. HN2025151], Zhengzhou Youth Science and Technology Talent Program [No. 20248651] and Postgraduate Education Reform and Quality Improvement Project of Henan Province [No. YJS2023JD67].

Institutional Review Board Statement: Ethical review and approval were waived for this study as it only involves the analysis of publicly available datasets, and no new data were collected from human participants.

Informed Consent Statement: Participant consent was waived as the data used in this study were obtained from publicly available EEG datasets, which were collected in accordance with relevant ethical guidelines and made available for research purposes.

Data Availability Statement: The original data presented in the study are openly available in https://datadryad.org/dataset/doi:10.5061/dryad.wh70rxwmv, accessed on 12 April 2026.

Conflicts of Interest: The authors declare no conflicts of interest.

References

1. Binnie, C.; Prior, P. Electroencephalography. *J. Neurol. Neurosurg. Psychiatry* **1994**, *57*, 1308–1319. [CrossRef]
2. Pfurtscheller, G.; Neuper, C. Motor imagery and direct brain-computer communication. *Proc. IEEE* **2001**, *89*, 1123–1134. [CrossRef]
3. Vialatte, F.-B.; Maurice, M.; Dauwels, J.; Cichocki, A. Steady-state visually evoked potentials: Focus on essential paradigms and future perspectives. *Prog. Neurobiol.* **2010**, *90*, 418–438. [CrossRef] [PubMed]
4. Jeannerod, M. The representing brain: Neural correlates of motor intention and imagery. *Behav. Brain Sci.* **1994**, *17*, 187–202. [CrossRef]
5. Invitto, S.; Faggiano, C.; Sammarco, S.; De Luca, V.; De Paolis, L.T. Haptic, virtual interaction and motor imagery: Entertainment tools and psychophysiological testing. *Sensors* **2016**, *16*, 394. [CrossRef]
6. Degenhart, A.D.; Bishop, W.E.; Oby, E.R.; Tyler-Kabara, E.C.; Chase, S.M.; Batista, A.P.; Yu, B.M. Stabilization of a brain–computer interface via the alignment of low-dimensional spaces of neural activity. *Nat. Biomed. Eng.* **2020**, *4*, 672–685. [CrossRef]
7. Xue, Z.; Zhang, Y.; Li, H.; Chen, H.; Shen, S.; Du, H. Instrumentation, measurement, and signal processing in electroencephalography-based brain–computer interfaces: Situations and prospects. *IEEE Trans. Instrum. Meas.* **2024**, *73*, 6504128.
8. Li, X.; Tang, X.; Liu, J.; Liu, Q.; Wang, H.; Liu, K. Parameter transfer and Riemannian space coordinate alignment for EEG intention recognition. *Biomed. Signal Process. Control* **2024**, *92*, 106044. [CrossRef]
9. Lotte, F.; Larrue, F.; Mühl, C. Flaws in current human training protocols for spontaneous brain-computer interfaces: Lessons learned from instructional design. *Front. Hum. Neurosci.* **2013**, *7*, 568. [CrossRef]
10. Saga, N.; Doi, A.; Oda, T.; Kudoh, S.N. Elucidation of EEG characteristics of fuzzy reasoning-based heuristic BCI and its application to patient with brain infarction. *Front. Neurorobot.* **2021**, *14*, 607706. [CrossRef]
11. Peng, F.; Li, M.; Zhao, S.-N.; Xu, Q.; Xu, J.; Wu, H. Control of a robotic arm with an optimized common template-based CCA method for SSVEP-based BCI. *Front. Neurorobot.* **2022**, *16*, 855825. [CrossRef] [PubMed]
12. Aarabi, A.; Kazemi, K.; Grebe, R.; Moghaddam, H.A.; Wallois, F. Detection of EEG transients in neonates and older children using a system based on dynamic time-warping template matching and spatial dipole clustering. *Neuroimage* **2009**, *48*, 50–62. [CrossRef] [PubMed]
13. Witkiewitz, K.; Wilson, A.D.; Pearson, M.R.; Hallgren, K.A.; Falk, D.E.; Litten, R.Z.; Kranzler, H.R.; Mann, K.F.; Hasin, D.S.; O'Malley, S.S. Temporal stability of heavy drinking days and drinking reductions among heavy drinkers in the COMBINE study. *Alcohol. Clin. Exp. Res.* **2017**, *41*, 1054–1062. [CrossRef]
14. Jiménez-Guarneros, M.; Fuentes-Pineda, G. Learning a robust unified domain adaptation framework for cross-subject EEG-based emotion recognition. *Biomed. Signal Process. Control* **2023**, *86*, 105138. [CrossRef]
15. Wan, Z.; Yu, Q.; Dai, W.; Li, S.; Hong, J. Data generation for enhancing EEG-based emotion recognition: Extracting time-invariant and subject-invariant components with contrastive learning. *IEEE Trans. Consum. Electron.* **2024**, *71*, 1371–1384. [CrossRef]
16. Müller, M. Dynamic time warping. In *Information Retrieval for Music and Motion*; Springer: Berlin/Heidelberg, Germany, 2007; pp. 69–84.
17. Huang, H.-C.; Jansen, B. EEG waveform analysis by means of dynamic time-warping. *Int. J. Bio-Med. Comput.* **1985**, *17*, 135–144. [CrossRef]
18. Zhou, F.; De la Torre, F. Generalized canonical time warping. *IEEE Trans. Pattern Anal. Mach. Intell.* **2015**, *38*, 279–294. [CrossRef]
19. Zhao, J.; Itti, L. shapeDTW: Shape dynamic time warping. *Pattern Recognit.* **2018**, *74*, 171–184. [CrossRef]
20. Soheily-Khah, S.; Marteau, P.-F. Sparsification of the alignment path search space in dynamic time warping. *Appl. Soft Comput.* **2019**, *78*, 630–640. [CrossRef]
21. Hong, J.Y.; Park, S.H.; Baek, J.-G. SSDTW: Shape segment dynamic time warping. *Expert Syst. Appl.* **2020**, *150*, 113291. [CrossRef]
22. Chemin, B.; Huang, G.; Mulders, D.; Mouraux, A. EEG time-warping to study non-strictly-periodic EEG signals related to the production of rhythmic movements. *J. Neurosci. Methods* **2018**, *308*, 106–115. [CrossRef]
23. Willett, F.R.; Avansino, D.T.; Hochberg, L.R.; Henderson, J.M.; Shenoy, K.V. High-performance brain-to-text communication via handwriting. *Nature* **2021**, *593*, 249–254. [CrossRef] [PubMed]
24. Williams, A.H.; Poole, B.; Maheswaranathan, N.; Dhawale, A.K.; Fisher, T.; Wilson, C.D.; Brann, D.H.; Trautmann, E.M.; Ryu, S.; Shusterman, R. Discovering precise temporal patterns in large-scale neural recordings through robust and interpretable time warping. *Neuron* **2020**, *105*, 246–259.e8. [CrossRef] [PubMed]
25. Song, M.; Gwon, D.; Jun, S.C.; Ahn, M. Signal alignment for cross-datasets in P300 brain-computer interfaces. *J. Neural Eng.* **2024**, *21*, 036007. [CrossRef] [PubMed]
26. Goudar, V.; Buonomano, D.V. Encoding sensory and motor patterns as time-invariant trajectories in recurrent neural networks. *eLife* **2018**, *7*, e31134. [CrossRef]
27. Anh, D.T.; Thanh, L.H. An efficient implementation of k-means clustering for time series data with DTW distance. *Int. J. Bus. Intell. Data Min.* **2015**, *10*, 213–232. [CrossRef]

28. Thuwajit, P.; Rangpong, P.; Sawangjai, P.; Autthasan, P.; Chaisaen, R.; Banluesombatkul, N.; Boonchit, P.; Tatsaringkansakul, N.; Sudhawiyangkul, T.; Wilaiprasitporn, T. EEGWaveNet: Multiscale CNN-based spatiotemporal feature extraction for EEG seizure detection. *IEEE Trans. Ind. Inform.* **2021**, *18*, 5547–5557. [CrossRef]
29. Lerogeron, H.; Picot-Clémente, R.; Rakotomamonjy, A.; Heutte, L. Approximating dynamic time warping with a convolutional neural network on EEG data. *Pattern Recognit. Lett.* **2023**, *171*, 162–169. [CrossRef]
30. Supakar, R.; Satvaya, P.; Chakrabarti, P. A deep learning based model using RNN-LSTM for the detection of schizophrenia from EEG data. *Comput. Biol. Med.* **2022**, *151*, 106225. [CrossRef]
31. Liu, S.; Wang, Z.; An, Y.; Zhao, J.; Zhao, Y.; Zhang, Y.-D. EEG emotion recognition based on the attention mechanism and pre-trained convolution capsule network. *Knowl.-Based Syst.* **2023**, *265*, 110372. [CrossRef]
32. Nejedly, P.; Kremen, V.; Lepkova, K.; Mivalt, F.; Sladky, V.; Pridalova, T.; Plesinger, F.; Jurak, P.; Pail, M.; Brazdil, M. Utilization of temporal autoencoder for semi-supervised intracranial EEG clustering and classification. *Sci. Rep.* **2023**, *13*, 744. [CrossRef] [PubMed]
33. Folgado, D.; Barandas, M.; Matias, R.; Martins, R.; Carvalho, M.; Gamboa, H. Time alignment measurement for time series. *Pattern Recognit.* **2018**, *81*, 268–279. [CrossRef]
34. Ames, K.C.; Churchland, M.M. Motor cortex signals for each arm are mixed across hemispheres and neurons yet partitioned within the population response. *eLife* **2019**, *8*, e46159. [CrossRef] [PubMed]
35. Wilson, G.H.; Stein, E.A.; Kamdar, F.; Avansino, D.T.; Pun, T.K.; Gross, R.; Hosman, T.; Singer-Clark, T.; Kapitonava, A.; Hochberg, L.R. Long-term unsupervised recalibration of cursor-based intracortical brain–computer interfaces using a hidden Markov model. *Nat. Biomed. Eng.* **2025**, *9*, 1–19. [CrossRef] [PubMed]
36. Xue, J. Handwriting with brain computer interface. In *Journal of Physics: Conference Series*; IOP Publishing: Bristol, UK, 2021; p. 042026.
37. Vry, M.-S.; Saur, D.; Rijntjes, M.; Umarova, R.; Kellmeyer, P.; Schnell, S.; Glauche, V.; Hamzei, F.; Weiller, C. Ventral and dorsal fiber systems for imagined and executed movement. *Exp. Brain Res.* **2012**, *219*, 203–216. [CrossRef]
38. Vincenzo, R.; Marianna, C.; Rossella, C.; Gianluca, D.F.; Andrea, G.; Daniele, G.; Gianluca, B.; Fabio, B.; Pietro, A. Beyond the lab: Real-world benchmarking of wearable EEGs for passive brain-computer interfaces. *Brain Inform.* **2026**, *13*, 3. [CrossRef]
39. Luo, Y.; Ke, W.; Lam, C.-T.; Im, S.-K. An accurate slicing method for dynamic time warping algorithm and the segment-level early abandoning optimization. *Knowl.-Based Syst.* **2024**, *300*, 112231. [CrossRef]
40. Cheng, C.; Zhang, Y.; Liu, L.; Liu, W.; Feng, L. Multi-domain encoding of spatiotemporal dynamics in EEG for emotion recognition. *IEEE J. Biomed. Health Inform.* **2022**, *27*, 1342–1353. [CrossRef]
41. Falini, A. A review on the selection criteria for the truncated SVD in Data Science applications. *J. Comput. Math. Data Sci.* **2022**, *5*, 100064. [CrossRef]
42. Abdi, H.; Williams, L.J. Principal component analysis. *Wiley Interdiscip. Rev. Comput. Stat.* **2010**, *2*, 433–459. [CrossRef]
43. Tošić, I.; Frossard, P. Dictionary learning. *IEEE Signal Process. Mag.* **2011**, *28*, 27–38. [CrossRef]
44. Williams, A.H.; Kim, T.H.; Wang, F.; Vyas, S.; Ryu, S.I.; Shenoy, K.V.; Schnitzer, M.; Kolda, T.G.; Ganguli, S. Unsupervised discovery of demixed, low-dimensional neural dynamics across multiple timescales through tensor component analysis. *Neuron* **2018**, *98*, 1099–1115.e8. [CrossRef]
45. McNeish, D.; Wolf, M.G. Dynamic fit index cutoffs for confirmatory factor analysis models. *Psychol. Methods* **2023**, *28*, 61. [CrossRef]
46. Atla, K.G.R.; Sharma, R. Motor imagery classification using a novel CNN in EEG-BCI with common average reference and sliding window techniques. *Alex. Eng. J.* **2025**, *120*, 532–546. [CrossRef]

Disclaimer/Publisher's Note: The statements, opinions and data contained in all publications are solely those of the individual author(s) and contributor(s) and not of MDPI and/or the editor(s). MDPI and/or the editor(s) disclaim responsibility for any injury to people or property resulting from any ideas, methods, instructions or products referred to in the content.